Article

The Directing Role of Aluminum in the Synthesis of PST-21 (PWO), PST-22 (PWW), and ERS-7 (ESV) Zeolites

Omer F. Altundal and German Sastre*

Read Online

ACCESS | Metrics & More | Article Recommendations | Supporting Information

ABSTRACT: Zeolites are a diverse class of crystalline microporous materials of, mainly, aluminosilicate chemical composition. Organic structure-directing agents (OSDAs) are generally utilized in zeolite synthesis to drive the outcome to a specific zeolite phase. In addition to OSDA, the presence and content of aluminum in the gel play a role in driving the synthesis under specific conditions. The structure-directing role of aluminum as well as fluoride in zeolite synthesis was explored through the analysis of three recently synthesized aluminosilicate zeolites, PST-21 (PWO), PST-22 (PWW), and ERS-7 (ESV), using a force field simulation approach. An updated and recently proposed method based on the calculation of "synthesis energy" is used to predict the stability of zeolites at pure-silica and aluminosilicate gel compositions, also able to include fluoride anions as well as OSDAs, and hence largely general. The results are not only demonstrating that the calculated structures with lowest "synthesis energy" correspond to those experimentally obtained under "standard" (meaning HF/SDA = 1) synthesis conditions but also that new structures obtained under the recently introduced "excess fluoride approach" are those which follow with energy slightly larger than the lowest, as calculated from the list of competing zeolites. With this method, we were able to rationalize the structure-directing effect of aluminum, in the presence of fluoride and OSDAs, in the synthesis of zeolites.
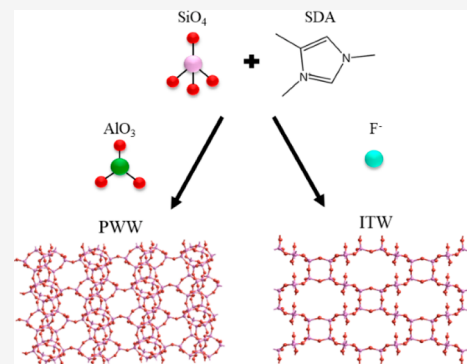
1. INTRODUCTION

Chemical disorder of Si and Al corner-sharing tetrahedra in zeolites is a key property that gives room to a large number of possibilities whose control leads to tuning the location and strength of Brønsted acid sites, SiO(H)Al, aka the catalytic properties.[1−3] Such disorder is only limited by the well-known Loewenstein rule enunciated in 1954:[4] "Whenever two tetrahedra are linked by one oxygen bridge, the center of only one of them can be occupied by aluminum; the other center must be occupied by silicon. ... Likewise, whenever two aluminum ions are neighbors to the same oxygen anion, at least one of them must have a coordination number larger than four, that is, five or six, towards oxygen". Also, the looser Dempsey rule suggests that the number of close aluminum such as Al−O−Si−O−Al must be minimized.[5]

Early computational work aimed to elucidate the Al distribution in zeolites was based on an exhaustive analysis of all possible Al locations for each given Si/Al ratio[6,7] studied either without or with taking into consideration the energy of each configuration through a force field approach. Since for most of the Si/Al ratios the number of possible Si, Al configurations is large and XRD does not allow one to distinguish Si and Al due to their similar number of electrons, it soon became of crucial interest to put forward experimental techniques providing accurate information about the location of Al. In some instances, XRD gives some indication of preferential Al location corresponding to larger T-O distance (T = tetrahedral atom,

Si, Al) since Al−O bonds (ca. 1.75 Å) are larger than Si−O bonds (ca. 1.61 Å). ^{29}Si NMR provides valuable information by allowing us to quantify the number of first T-neighbors of each Si type, Si(n-Al), with n = 0−4.[8] This has been recently employed, together with inelastic neutron scattering (INS) and periodic DFT calculations, to elucidate the Si, Al distribution of LTA zeolites with high (40)[9] and low (5)[10] Si/Al ratios, and also more recently using IR and 2D MAS NMR spectroscopy plus DFT calculations.[11] A similar theoretical approach, although without including zeolite framework relaxation upon Al substitution has been presented by Jeffroy et al.,[12] based on an exhaustive Monte Carlo approach that makes an analysis of all Si, Al distributions and determines average properties based on equilibrium configurations.

Conventional ^{27}Al MAS NMR is unable to characterize different Al species, since quadrupolar Al interactions lead to peak broadening. High sample spin rates and large r number of scans, together with ^{27}Al multiple quantum (MQ) MAS NMR may allow differentiation of the peaks corresponding to each Al
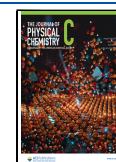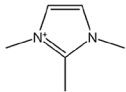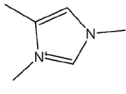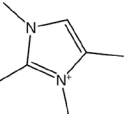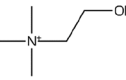
Table 1. Names and Structures of the SDA Molecules Considered in This Study and Zeolite Phases Obtained by Using Them under Pure-Silica and Aluminosilicate Conditions[a]

SDA	Name	Pure-Silica	Aluminosilicate	Structure
SDA1	1,2,3-trimethylimidazolium	ITW, MTW	NON, PWO, RTH	
SDA2	1,3,4-trimethylimidazolium	ITW, TON	FER, PWW	
SDA3	1,2,3,4-tetramethylimidazolium	ITW, STW	PWW, RTH	
SDA4	Choline	AST, MTN, NON	ESV, FER, RUT	

[a]References and more details are given in Table S1 (Supporting Information).

crystallographic site. Notably, Sklenak et al.[13] prepared a large number of ZSM-5 samples (Si/Al = 14−45) and were able to distinguish the Al population of the 24 different crystallographic positions using ^{27}Al MQ MAS NMR spectra, and periodic quantum/classic calculations. A similar strategy in the group of Yokoi and co-workers, using high-resolution ^{27}Al MAS NMR technique, allowed them to distinguish whether the different Al peaks belong to the different types of micropores in zeolite structures such as MFI[14] and MSE.[15] Further, the authors analyze samples of the same topology and same Si/Al, obtained with different organic structure directing agents (OSDAs), to demonstrate how each OSDA generates a different Al distribution. With an appropriate selection of OSDAs, also combined with inorganic SDAs, it is possible to generate aluminum and, hence, Brønsted sites preferentially located in specific micropores. The implications and fine control of these effects in catalysis have been exploited recently by several groups.[16−26] All this knowledge arises importantly from the initial discovery by Shantz et al.[27] of geometrical relations between the positive charge of OSDAs and the negative charge of the $[AlO_{4/2}]^-$ tetrahedra in ZSM-12 zeolite, suggesting that the distribution of acid sites can be controlled using OSDAs with different charge distributions. This was soon confirmed in our group using a computational approach that was able to suggest a Si, Al distribution in ZSM-18 synthesized with trispyrrolidinium[28] as well as ITQ-7 synthesized with 1,3,3-trimethyl-6-azonium-tricyclo[3.2.1.4^{6,6}]dodecane hydroxide,[29] in both cases not in disagreement with experimental findings from XRD (T−O distances) and the infrared spectrum (O−H stretching region), respectively. Wang et al.[30] combined DFT calculations with molecular dynamics simulations to investigate the effect of OSDA orientation on the Al distribution in CHA type zeolites by modeling every possible OSDA orientation and Al distribution in CHA zeolite. Their energetic analysis showed that total energies are sensitive to Al−Al proximity and that Al pairs in 8-rings were favored since they are closer to the quaternary ammonium center of N,N,N-trimethyl-1-adamantyl ammonium cations. Recent work by Rubeš et al.[31] has also used infrared OH stretching spectra to validate the computational work on FER, TON, CHA, and IFR. The above work on ZSM-18 allows the effects of framework flexibility and zeolite-OSDA interactions to be separated through the calculation of the

relative energetic penalties resulting from introducing Al in the different crystallographic position by using the Mott−Littleton methodology for defects. The results for ZSM-18 show that the less favorable Al position is in fact the most populated due to the dominant effect of the Al-OSDA electrostatics. Instead of separating the effects of intrinsic Al stability (in the absence of OSDA) plus the effect of zeolite-OSDA interactions, most recent work only focuses on the analysis of total energies of the different Si, Al configurations in the zeolite-OSDA system. More recent work on finding Al distributions in zeolites include that by Muraoka et al.[32] which deals with IFR obtained with, among others, N-benzyl-DABCO and N-benzyl-quinuclidinium, which only differ in N vs CH atoms, respectively. This small difference, in a tight microporous packing, is enough to produce a larger population probability for Al3 when N-benzyl-DABCO is used as OSDA instead of N-benzyl-quinuclidinium, in agreement with ^{27}Al MQMAS NMR results.

An excellent recent computational study by Antúnez-García et al.[33] employs periodic DFT calculations to analyze how the stable locations of Al change across the 4 crystallographic sites of mordenite from high Si/Al = 40 down to low Si/Al = 5. The study was able to justify the rule of one Al occupancy for each ζ-cage (t-tes, $[5^4]$) in the framework, which explains the limit of maximum Al content at Si/Al = 5.

While the topic of Si, Al ordering in a zeolite is a topic widely studied, as well as the role of OSDAs in the synthesis of zeolites,[15,19,34−38] the reasons why (or if) the aluminum contributes to stabilize such a zeolite phase is a less explored aspect, and this is the aim of the present study. Following the idea of our previous work regarding the roles of fluoride[39] and aluminum[40] as SDAs in the synthesis of zeolites, we now try to compare the role of aluminum and fluoride on the synthesis of recently synthesized aluminosilicate zeolites PST-21 (PWO), PST-22[41] (PWW), and ERS-7[42] (ESV) by selecting certain specific cases in which different zeolites are obtained using the same OSDA when the synthesis gel has a silicate or aluminosilicate chemical composition. PST-21 and PST-22 both consist of nonjointly connected *bre* composite building units, which are synthesized under excess fluoride conditions using 1,2,3-trimethylimidazolium, 1,3,4-trimethylimidazolium, and 1,2,3,4-tetramethylimidazolium as OSDA molecules, respectively. The small pore, one-dimensional zeolite, ERS-7 is

synthesized using choline, again under excess fluoride conditions.

2. COMPUTATIONAL METHODS

2.1. SDA and Competing Phase Selection. Our aim was to investigate, in detail, the structure-directing effect of aluminum in the synthesis of these zeolites and how the synthesis products change under similar synthesis conditions when synthesis gels contain either silicate or aluminosilicate. To achieve that, we searched for recently synthesized aluminosilicate zeolites using the Database of Zeolite Structures created by the International Zeolite Association,[43] which returned seven zeolite phases: PTO, PTT, PTY, PWN, PWO, PWW, and ESV. Since we want to focus on the structure-directing effects of framework Al atoms and F^- anions specifically, the zeolite phases that are synthesized using inorganic cations (e.g., Na^+, K^+) and seed crystals were removed, which left us with three aluminosilicate zeolite phases: PWO, PWW, and ESV. Interestingly these zeolites have, so far, not been obtained as pure silica. Using the information from the publications of these three zeolites, the OSDAs employed for the syntheses were identified, and a list of four OSDAs was obtained. To determine the competing zeolite phases for each OSDA molecule, an exhaustive literature search using the Organic Structure Database (OSDB)[44] was performed, which led to 52 publications. Similar to our previous work,[40] the publications that include (i) synthesis in the presence of seed crystals, (ii) synthesis in the presence of inorganic cations, (iii) synthesis of germanosilicates, and (iv) synthesis of MFI, FAU, and MOR phases, since they are easy to obtain without an SDA present, were removed from the records to focus on the structure-directing effect of Al and F^-. In the end, seven publications fit those criteria.

From the information gathered from the remaining publications, a table was generated containing the relevant synthesis information, such as the presence of Al atoms in the synthesis, Si/Al, and HF/SDA, and zeolite obtained for each OSDA molecule (Table S1). The most relevant information is presented in Table S1, with names and structures of the OSDA molecules as well as the competing zeolite phases for both aluminosilicate and pure-silica gels is given in Table 1. The resulting product of the synthesis depends on various properties of the synthesis gel such as Si/Al and HF/SDA. Table 2 is given in order to facilitate comparison of our computational results with synthesis experiments by Jo et al.[41] and Bae et al.[42] at various gel conditions, using the "excess fluoride approach".

2.2. Force Field Simulation Details. Similar to our previous studies,[39,40] to find the optimal position of SDA molecules and fluoride anions (in the case of synthesis in fluoride media) inside the zeolite cavities, zeoTsda software was employed.[45] zeoTsda software works by finding the most favorable location of SDAs, at full loading, on a given pure silica zeolite through Monte Carlo + Lattice Energy Minimization (MC+LEM) using the General Utility Lattice Program (GULP).[46] Then, for the optimized zeo(Si)-SDA system, 100 Al distributions are generated with zeoTAl software[9] (a modified version of zeoTsites software), with an Al content that is selected so as to counteract the SDA loading found previously. All of the Al distributions generated follow the Lowenstein rule. Each of these 100 zeo(Si,Al)-SDA unit cells is energy minimized using the previously found SDA location as the initial location and the corresponding energies are compared so that the zeo(Si,Al)-SDA configuration with the lowest energy

Table 2. Experimentally Synthesized Zeolite Phases, Using the SDA Molecules Considered in This Work, Taken from Studies by Jo et al.[41] (SDA1, SDA2, SDA3) and Bae et al.[42] (SDA4)[a]

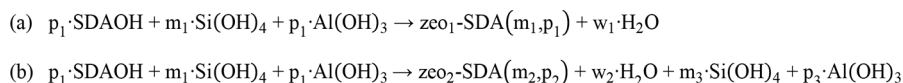| SDA	Si/Al	HF/SDA			
		0.5	1.0	2.0	3.0
SDA1	10	RTH+ITW	RTH+ITW	PWO	ITW
	∞	A	ITW	ITW	ITW
SDA2	10	FER	FER+U	PWW	TON+A
	∞	ITW+TON	ITW	ITW	D
SDA3	10	RTH	RTH+ITW	PWW	PWW+A
	20	RTH+ITW	ITW+RTH	PWW+ITW	ITW
	∞	STW+A	STW	ITW	ITW
SDA4	10	FER+RUT	FER	ESV	A
	∞	MTN+AST	AST	NON+U	A

[a]A, D, and U denote amorphous, dense, and unknown phases, respectively.

is selected. This method for finding the Al distribution with the lowest energy was proven efficient in one of our previous studies[10] where the computationally modeled LTA zeolite had similar ^{29}Si MAS NMR and INS spectra with the experimental structure. In the first stage, when using zeoTsda, it is possible to consider the possibility of adding fluoride anions to the system, in which case its most stable location is also found by using the same MC+LEM approach. When no fluoride is selected, the atomic charges of the SDA atoms are corrected by a special procedure, so that the overall charge becomes zero. This is the current approach for pure silica systems mimicking the synthesis in hydroxide media, which in the near future will be replaced by a zeolite containing defects.

In molecular simulations, the nonbonded two-body interactions between SDA molecules as well as zeolite atoms (Al, O, Si) were described by Lennard-Jones potential with a cutoff radius of 12 Å. The potential parameters of the SDA atoms were taken from Oie et al.[47] An overall cationic charge (+1) was assigned to the SDA molecules to compensate for the anionic charge (−1) of fluoride anions and Al-(O_4)-$(SiO_{3/2})_4$ units. The charge distribution of the SDAs along with $Si(OH)_4$, $Al(OH)_3$, and H_2O molecules was done by a charge equilibration approach.[48] The charges of zeolite atoms were taken from the force field by Bushuev and Sastre (BS),[49] where charges of Si and O atoms for the central SiO_4 tetrahedra in Si-(O_4)-$(SiO_{3/2})_4$ units are 2.1 and −1.05, respectively, corresponding to an overall zero charge, while the charges of Al and O atoms for the central AlO_4 tetrahedra in Al-(O_4)-$(SiO_{3/2})_4$ units are 1.575 and −1.16875, respectively, giving an overall −1 charge ($1.575 − 1.16875 \times 4 + 2.1 \times 4 − 1.05 \times 6$). The Ewald summation method was employed for the incorporation of long-range electrostatic interactions.[50] The Al content of zeolites was specified according to the Si/Al ratio of the synthesis gel such that the Si/Al ratios of the zeolites were similar to that of the synthesis gel. Therefore, when the number of Al-(O_4)-$(SiO_{3/2})_4$ units of the zeo-SDA system is lower than the number of SDA molecules, the remaining cationic charge is compensated by F^- anions. The preferential locations of the F^- anions for each zeolite are given in the relevant section in the Supporting Information.

2.3. Synthesis Energy Calculations. In this manuscript, as well as our recent previous study,[40] we compare the stabilities of zeolites according to their "synthesis energy", a parameter we

Scheme 1. Synthesis Reactions of Aluminosilicate Zeolites

(a) $p_1 \cdot \text{SDAOH} + m_1 \cdot \text{Si(OH)}_4 + p_1 \cdot \text{Al(OH)}_3 \rightarrow \text{zeo}_1\text{-SDA}(m_1, p_1) + w_1 \cdot \text{H}_2\text{O}$

(b) $p_1 \cdot \text{SDAOH} + m_1 \cdot \text{Si(OH)}_4 + p_1 \cdot \text{Al(OH)}_3 \rightarrow \text{zeo}_2\text{-SDA}(m_2, p_2) + w_2 \cdot \text{H}_2\text{O} + m_3 \cdot \text{Si(OH)}_4 + p_3 \cdot \text{Al(OH)}_3$

recently derived based on the fact that two different zeolites can be synthesized using the same reactants.

In Scheme 1, the same reactants are used to synthesize two zeolites. Employing the same reactants, one zeolite (zeo$_1$) is obtained with Si/Al = m_1/p_1 with water as a product, whereas the other zeolite (zeo$_2$) is synthesized with Si/Al = m_2/p_2 giving excess Si and Al monomers (m_3 and p_3). Since both reactions have the same reactants, the energetic stability of the products can be directly compared to each other. A detailed analysis of the energies of both equations (see ref 40. and Supporting Information section S2) results in the following equation which quantifies the stability of zeolite-SDA pairs from their synthesis reactions.

$$E_{\text{syn}} = E_{\text{zeo-SDA-F}} + 2 \cdot E_{\text{H}_2\text{O}} - (p - q)/(m + p) \cdot$$
$$(E_{\text{SDAOH}} + E_{\text{Al(OH)}_3}) - q/(m + p) \cdot E_{\text{SDAF}}$$
$$- (m + q)/(m + p) \cdot E_{\text{Si(OH)}_4} \qquad (1)$$

E_{syn} is the "synthesis energy" which represents the total energy of reaction for the synthesis of zeolites, $E_{\text{zeo-SDA-F}}$ is the energy of zeo-SDA pair with a set Si/Al, and E_{SDAOH} is the energy of SDA which is neutralized with an OH$^-$ group. "p" and "q" represent the total number of SDA molecules employed and the number of F$^-$ anions in the framework, respectively, in equation 1. The number of Al atoms in the framework is equal to "$p - q$" to achieve the charge balance in the structure. Finally, to be consistent with the total number of tetrahedral atoms with synthesis energy equation of our previous publication,[40] we set the number of Si as "$m + q$", leading to a total number of $(m + q) + (p - q) = m + p$ total tetrahedral atoms (Si + Al). Because of their energetic contribution to the oligomerization and ring closure processes during zeolite synthesis, the energies of H$_2$O, Si(OH)$_4$, and Al(OH)$_3$ (Table S2) are incorporated in equation 1.

The synthesis product obtained by each SDA using pure-silica and aluminosilicate gel can be anticipated based on the E_{syn} values of all the competing phases, selecting the zeolite phase with the lowest E_{syn} value as the most stable.

3. RESULTS AND DISCUSSION

3.1. Synthesis Energies of Zeolites Using SDA1. The synthesis energies of possible aluminosilicate phases obtained using SDA1 with a synthesis gel corresponding to Si/Al of 10 are given in Table 3. Out of five total competing zeolite phases (Table 1), we excluded NON for the calculations since by allowing a maximum loading of 4 SDA1 in a unit cell of 88 T atoms, this leads to a maximum aluminum content of 84/4 = 21, and hence it is not possible to reach Si/Al = 10. The four remaining competing phases (RTH, ITW, PWO and MTW) could be synthesized with a Si/Al close to 10. From these four zeolites, RTH is calculated to have the lowest E_{syn} value of −1.406 eV/TO$_2$. This is in agreement with the experimental study of Jo et al.[41] (Table 2) as RTH is the main synthesis product at a gel composition of Si/Al = 10 and HF/SDA = 0.5 and 1.0 using SDA1.

Table 3. "Synthesis Energies" of Aluminosilicate Phases Obtained Using SDA1 with Si/Al of ca. 10 in the Synthesis Gel[a]

SDA	Zeolite	m	p	Si/Al	Total energy (eV/TO$_2$)	E(syn) (eV/TO$_2$)
SDA1	RTH	28	4	7	−39.708	−1.406
SDA1	ITW	22	2	11	−40.038	−1.006
SDA1	PWO	18	2	9	−39.877	−1.137
SDA1	MTW	52	4	13	−40.055	−0.814

[a]"m" and "p" represent the number of Si and Al atoms, respectively, in the unit cell.

To investigate the driving force for the synthesis of aluminosilicate and pure-silica zeolites, we calculated the van der Waals energies between zeolite-SDA pairs in Tables S3 and S4, respectively. zeo-SDA energies per SDA molecule give an indication of how well an SDA molecule fits into the cavities of zeolites, whereas zeo-SDA energies per T atom specify, in addition to the previous concept, the extent of the SDA packing. Both concepts contribute to stabilizing the corresponding zeolite phase. In the case of SDA1-RTH, the zeo-SDA energy per SDA molecule ($E_{\text{zeo-SDA}}^{\text{vdW}}$ = −0.755 eV/SDA, Table S3) implies that SDA1 does not have the best fit in RTH cavities. However, due to a favorable packing of two SDAs per zeolite cage, RTH has the lowest zeo-SDA van der Waals energy per T atoms ($E_{\text{zeo-SDA}}^{\text{vdW}}$ = −0.094 eV/TO$_2$), which contributes to the synthesis of aluminosilicate RTH. Moreover, RTH zeolite allows incorporation of a higher number of Al atoms to the framework, with more favorable incorporation energy than Si atoms, as demonstrated in our previous study.[40]

After RTH, the second most favorable synthesis energy is calculated for the PWO phase (−1.137 eV/TO$_2$), which is observed as the experimental synthesis product when the fluoride concentration in the gel increases (HF/SDA = 2.0, Table 2). Recently, Bae and Hong elucidated that the excess fluoride in aluminosilicate zeolite synthesis acts as a mineralizing agent accelerating the crystallization phase while also affecting the Al distribution in zeolites.[51] Therefore, under excess fluoride conditions, new zeolite phases that are not feasible under lower fluoride concentrations in the gel can be synthesized. Thus, it was possible to synthesize PWO using SDA1 at high fluoride concentration, even though the synthesis energy of PWO (−1.137 eV/TO$_2$) is not the most favorable among the competing zeolite phases. Hence, from the viewpoint of synthesis energies, the excess fluoride route allows the synthesis of phases with energy higher than that of the most stable.

When pure silica conditions were considered in the synthesis using SDA1 (Table 4), ITW became the preferred zeolite phase with an E_{syn} value of −0.359 eV/TO$_2$. This is in fact supported by the experimental studies that identify ITW as the synthesis product of pure silica synthesis under fluoride media using SDA1 (Table 2). There are two main reasons why ITW is obtained as the only pure silica product using SDA1: (i) Due to their shape, rigidity and hydrophobicity, small methylimidazo-lium cations, such as SDA1, are very selective for ITW zeolite.[52] The good fit between SDA1 and ITW cavities is also supported by the favorable zeo-SDA van der Waals energy of −1.141 eV/

Table 4. "Synthesis Energies" of Pure Silica Phases Obtained Using SDA1[a]

SDA	Zeolite	m	q	Si/Al	Total energy (eV/TO$_2$)	E(syn) (eV/TO$_2$)
SDA1	RTH	28	4	∞	−40.844	−0.307
SDA1	ITW	22	2	∞	−40.881	−0.359
SDA1	PWO	18	2	∞	−40.727	−0.199
SDA1	MTW	52	4	∞	−40.705	−0.188
SDA1	NON	84	4	∞	−40.654	−0.146

[a]"$m + q$" and "q" represent the number of Si and F atoms, respectively, in the unit cell.

SDA molecule between SDA1 and ITW in Table S4. (ii) ITW is a zeolite that contains double four rings (D4R), which are known to be favorably formed in the presence of fluoride.[53] Due to the presence of D4Rs, ITW is prone to being a pure silica zeolite under fluoride media even when the synthesis gel contains aluminum, to the extent that the ITW zeolite synthesized with the, so far, highest Al content only had Si/Al ratio of 70.[54]

3.2. Synthesis Energies of Zeolites Using SDA2. SDA2 is an isomer of SDA1 in which the methyl chain at the second carbon is substituted to the fourth carbon. Even though molecular volume and conformational rigidity of the two molecules are similar, they have different shapes, which leads to different competing aluminosilicate phases for both SDA molecules.[41,52] Table 5 shows the synthesis energies of

Table 5. "Synthesis Energies" of Aluminosilicate Phases Obtained Using SDA2 with Si/Al of ca. 10 in the Synthesis Gel[a]

SDA	Zeolite	m	p	Si/Al	Total energy (eV/TO$_2$)	E(syn) (eV/TO$_2$)
SDA2	FER	32	4	8	−39.879	−1.283
SDA2	ITW	22	2	11	−40.057	−0.987
SDA2	PWW	36	4	9	−39.884	−1.099

[a]"m" and "p" represent the number of Si and Al atoms, respectively, in the unit cell.

competing aluminosilicate zeolite phases when SDA2 is utilized in a synthesis gel with Si/Al = 10. FER, ITW, and PWW were identified as possible synthesis products with a Si/Al ratio close to 10 when SDA2 is used. Out of the three competing phases, FER is the preferred synthesis product according to the synthesis energies ($E_{\text{syn,FER}} = -1.283$ eV/TO$_2$) which agrees with the literature where FER is the synthesis product for SDA2 at lower fluoride concentrations (Table 2). The ability to accommodate more Al atoms per Si atom and a good fit of SDA in the 10-ring channels make FER the most favorable zeolite among its competitors. When the fluoride concentration increases (HF/SDA = 2.0), the synthesis product becomes PWW, which is correctly calculated to be the second most favorable zeolite phase according to its synthesis energy ($E_{\text{syn,PWW}} = -1.099$ eV/TO$_2$). Hence, again, increasing the HF/SDA ratio leads to the synthesis of less energetically stable zeolites.

At pure-silica conditions (Table 6), SDA2 is highly selective for ITW similar to its isomer, SDA1, due to the good fit of SDA molecules in ITW cavities $E_{\text{zeo-SDA}}^{\text{vdW}} = -1.157$ eV/SDA, Table S4) and the presence of D4Rs in the ITW structure favoring pure-silica zeolite. The selectivity of SDA2 for pure-silica ITW is accurately calculated as ITW has the lowest synthesis energy among all of the possible zeolite phases in competition ($E_{\text{syn,ITW}}$

Table 6. "Synthesis Energies" of Pure Silica Phases Obtained Using SDA2[a]

SDA	Zeolite	m	q	Si/Al	Total energy (eV/TO$_2$)	E(syn) (eV/TO$_2$)
SDA2	FER	32	4	∞	−40.842	−0.275
SDA2	ITW	22	2	∞	−40.887	−0.339
SDA2	PWW	36	4	∞	−40.733	−0.173
SDA2	TON	46	2	∞	−40.670	−0.151

[a]"$m + q$" and "q" represent the number of Si and F atoms, respectively, in the unit cell.

= −0.339 eV/TO$_2$). In the experiments, pure-silica TON was also seen as a side product at HF/SDA = 0.5. However, Rojas et al.[52] indicated that high framework density TON phase transforms *in situ* to ITW; therefore, TON is not considered a stable pure-silica synthesis product using SDA2.

3.3. Synthesis Energies of Zeolites Using SDA3. The last imidazolium cation we considered in this study is SDA3, a molecule slightly larger than SDA1 and SDA2 (one extra methyl group). Four zeolite phases were identified to be competing as aluminosilicate phases obtained using SDA3 in a synthesis gel with Si/Al = 10, namely, ITW, PWW, RTH, and STW (Table 7).

Table 7. "Synthesis Energies" of Aluminosilicate Phases Obtained Using SDA3 with Si/Al of 10 in the Synthesis Gel[a]

SDA	Zeolite	m	p	Si/Al	Total energy (eV/TO$_2$)	E(syn) (eV/TO$_2$)
SDA3	ITW	22	2	11	−40.008	−0.987
SDA3	PWW	36	4	9	−39.870	−1.143
SDA3	RTH	28	4	7	−39.672	−1.386
SDA3	STW	54	6	9	−39.772	−1.045

[a]"m" and "p" represent the number of Si and Al atoms, respectively, in the unit cell.

Out of these four zeolites, RTH has the most favorable synthesis energy of −1.386 eV/TO$_2$, in accordance with the experiments where RTH was the main synthesis product at lower fluoride concentrations (Table 2). The synthesis of RTH zeolite using SDA3 can be explained by a high degree of aluminum lattice substitution, which is energetically favorable. Moreover, even though the zeo-SDA energy between SDA3 and RTH is not the most favorable ($E_{\text{zeo-SDA}}^{\text{vdW}} = -0.100$ eV/TO$_2$, Table S3), it is not far from the zeo-SDA energy between SDA3 and PWW ($E_{\text{zeo-SDA}}^{\text{vdW}} = -0.105$ eV/TO$_2$), which indicates a good packing of SDA3 molecules in RTH cavities. As the fluoride content in the synthesis gel increases (HF/SDA = 2.0 and 3.0), RTH is replaced by PWW as the final product, which was correctly identified as the second most favored zeolite phase according to its synthesis energy ($E_{\text{syn,PWW}} = -1.143$ eV/TO$_2$). Therefore, the rule proposed that increasing HF/SDA allows us to obtain less stable phases is again followed.

For SDA3, we also calculated the synthesis energies of aluminosilicate phases obtained while using a synthesis gel with Si/Al = 20 (Table S7), in order to compare with the corresponding experimental results in Table 2. Similar to the results of synthesis with Si/Al = 10, RTH is the preferred zeolite phase at Si/Al = 20, with the lowest synthesis energy ($E_{\text{syn,RTH}} = -0.823$ eV/TO$_2$, Table S7), and RTH is in fact observed in the experimental results with HF/SDA values of 0.5 and 1.0 (Table 2). But then, as the fluoride content increases, also the less energetically favorable products appear, ITW and PWW (−0.666 and −0.685 eV/TO$_2$ respectively, Table S7).

According to these arguments, ITW should not be observed at low HF/SDA contents, in apparent contradiction to the experimental results in Table 2. But, as said above, it is unlikely that ITW was synthesized with Si/Al ca. 20, since an exhaustive study reported that ITW could not be obtained with a larger aluminum content than that corresponding to Si/Al = 70.[54] In the study by Jo et al.[41] cited in Table 2, the Si/Al of the ITW phase is not explicitly indicated.

The synthesis energies of zeolite phases in competition using SDA3 in a pure-silica synthesis gel are given in Table 8. Just like

Table 8. "Synthesis Energies" of Pure Silica Phases Obtained Using SDA3[a]

SDA	Zeolite	m	q	Si/Al	Total energy (eV/TO$_2$)	E(syn) (eV/TO$_2$)
SDA3	ITW	22	2	∞	−40.857	−0.358
SDA3	RTH	28	4	∞	−40.742	−0.239
SDA3	PWW	36	4	∞	−40.727	−0.226
SDA3	STW	54	6	∞	−40.760	−0.260

[a]"$m + q$" and "q" represent the number of Si and F atoms, respectively, in the unit cell.

the other imidazolium-based SDAs (SDA1 and SDA2) in this study, SDA3 also directs the synthesis to ITW. However, the bulkier SDA3 molecule also leads the synthesis to pure-silica STW, a 3-D large pore zeolite with D4Rs, at low fluoride contents (HF = 0.5 and 1.0, Table 2). According to the calculated synthesis energies, ITW is favored with an E_{syn} value of −0.358 eV/TO$_2$, whereas STW has the second lowest synthesis energy with an E_{syn} = −0.260 eV/TO$_2$. Both structures contain D4Rs in the framework which are favored by the presence of fluoride anions. The synthesis of ITW is also favored because of the excellent fit between SDA3 and ITW cavities as indicated by the zeo-SDA van der Waals energy of the SDA3-ITW complex ($E_{zeo\text{-}SDA}^{vdW}$ = −1.313 eV/TO$_2$, Table S4).

3.4. Synthesis Energies of Zeolites Using SDA4. Finally, the synthesis energies of the competing zeolite phases when SDA4 is utilized in a synthesis gel with Si/Al = 10 are given in Table 9. FER is calculated to be the preferred zeolite phase with

Table 9. "Synthesis Energies" of Aluminosilicate Phases Obtained Using SDA4 with Si/Al of 10 in the Synthesis Gel[a]

SDA	Zeolite	m	p	Si/Al	Total energy (eV/TO$_2$)	E(syn) (eV/TO$_2$)
SDA4	FER	32	4	8	−40.266	−1.008
SDA4	RUT	32	4	8	−40.257	−0.999
SDA4	AST	36	4	9	−40.221	−0.840
SDA4	ESV	44	4	11	−40.306	−0.740

[a]"m" and "p" represent the number of Si and Al atoms, respectively, in the unit cell.

a synthesis energy of −1.008 eV/TO$_2$ followed closely by RUT (E_{syn} = −0.999 eV/TO$_2$). This is in accordance with the experimental study of Bae et al.[42] where FER and RUT are the synthesis products at lower fluoride concentrations when SDA4 is utilized in aluminosilicate media, with FER being the main product (Table 2). In fact, Lee et al.[55] also stated that RUT was always obtained as an impurity using SDA4 with a very small amount of Na$^+$ present. The experimental synthesis data indicate that ESV can be synthesized under excess fluoride concentration (HF/SDA = 2.0); however, it was not possible to explain this from the synthesis energy of ESV. Our prediction is that AST

should be obtained at lower HF/SDA than ESV since the corresponding calculated synthesis energies are −0.840 and −0.740 eV/TO$_2$, and according to the previous results, we established the rule that zeolite phases of decreasing stability are obtained at increasing values of HF/SDA. Our prediction would be that AST should be obtained at values of HF/SDA larger than 1.0 (at which the most stable phase, FER, is observed) and lower than 2.0 (at which the less stable phase, ESV, is observed). Since this information is not present in the experiments reported in Table 2, we do not have, currently, enough information to try to explain why the calculated synthesis energy of ESV is higher than that of AST in the aluminosilicate composition (Table 9). Nevertheless, the experiments at HF/SDA = 1.0 indicate (Table 1 of ref 42) that AST was obtained at Si/Al = 20, hence hinting that this phase could also be obtained at HF/SDA = 1.5 and Si/Al ca. 9, according to our prediction.

SDA4 is the least selective SDA molecule in this study when pure-silica synthesis is considered since it led the synthesis to three different zeolite phases (MTN, AST, and NON) depending on the fluoride concentration of the synthesis gel. However, AST stands out from the others as it can be synthesized in the two syntheses with low fluoride content (HF/SDA= 0.5 and 1.0, Table 2). This is correctly calculated using the synthesis energy method as AST is the most favored pure-silica zeolite phase when SDA4 is utilized, with an E_{syn} value of −0.168 eV/TO$_2$ (Table 10). The main factors behind

Table 10. "Synthesis Energies" of Pure Silica Phases Obtained Using SDA4[a]

SDA	Zeolite	m	q	Si/Al	Total energy (eV/TO$_2$)	E(syn) (eV/TO$_2$)
SDA4	AST	36	4	∞	−41.265	−0.168
SDA4	ESV	44	4	∞	−41.014	−0.018
SDA4	FER	32	4	∞	−41.241	−0.077
SDA4	MTN	128	8	∞	−40.855	−0.008
SDA4	NON	84	4	∞	−40.828	−0.062
SDA4	RUT	32	4	∞	−41.252	−0.088

[a]"$m + q$" and "q" represent the number of Si and F atoms, respectively, in the unit cell.

the preferred synthesis of pure-silica AST using SDA4 are the D4R units in the zeolite structure, which is favored by fluoride anions, and the small size of the SDA which allows it to have a good fit in the small cavities of the clathrasil AST.

Overall, total energies of the zeo-SDA system (shown in Tables 3−10) were not explicitly employed in the comparison between calculated and experimental results, unlike an older energetic analysis in our group.[39] Since the recent introduction of the equations related to synthesis energies in a previous study,[40] as well as in this study, it has become possible to compare energies in a more realistic way, regardless not only the zeolite phase but also the chemical composition of the final material. Synthesis energy, on the other hand, requires the value of total energy for its calculation as well as other energetic terms whose calculation is simple, and hence it gives a wider picture of the thermodynamics of the system than total energy.

It is also important to recall that a number of approximations have been done. For instance, solvation energies were not considered. Charged SDA molecules are not incorporated into the zeolite coming from the "gas phase" (isolated molecule), as implied in our calculations, but rather they are solvated by water molecules, and the same argument also holds for fluoride anions.

Another approximation, for the particular case of pure silica zeolites, is that by considering a perfect silica crystal (electrically neutral), the SDA charge had to be "neutralized" (by changing atomic charges so that the overall charge becomes neutral), while, instead, the more correct approach of considering zeolite defects (silanol and siloxy) has not yet been introduced. A continuation of our recent study of defects[56] is expected to allow further insights into the role of defects in the processes being studied here. Sources of silica and alumina are also another aspect that has so far not been introduced in the synthesis equations as well as free energies in order to understand the role of entropy during the synthesis. Finally, the accuracy of the computational method was somehow addressed in our previous study,[40] with period DFT results being very similar to those obtained using the current force field. Other effects such as pH and water/silica ratio can hardly be introduced in this type of calculation but have been considered in alternative computational ways of addressing the synthesis of zeolites, based on classical nucleation theory and molecular dynamics simulations, with promising results.[57,58]

We are aware that in the excess fluoride approach, it is possible to obtain the same zeolite at increasing fluoride content, and in that case, the Al distributions are different. We are currently not capable of simulating this with our methods, but we can suggest that the number or location of defects might be different in each case, although it is widely known that the fluoride route leads to almost no defects. This topic will be addressed in the future.

In this study, only the Al distribution with the lowest energy for each zeo-SDA pair was used. In other words, "synthesis energies" for different Al–Al distributions within the same zeo-SDA pair were not calculated.

4. CONCLUSIONS

Synthesis energies have been introduced for aluminosilicate zeolites with fluoride, and a general way to calculate them over the full range of silica and aluminosilicate with and without fluoride is now possible. This allows ranking zeolite stabilities among competing phases with those having the lowest synthesis energy being the main prediction of synthesis.

Recent work in the group of Hong demonstrated that new zeolite phases may appear when using the fluoride route at HF/SDA ratios larger than the usual values, close to 1, in what is called the "excess fluoride approach". Our calculations suggest that increasing larger values of HF/SDA stabilize zeolite phases with increasingly higher synthesis energy. The force field employed in this study seems to be accurate enough to predict or justify the zeolite phases obtained with a given SDA throughout the synthesis gel composition going from pure silica to aluminosilicate. The computational results allow us to predict the more likely amount of aluminum (also known as Si/Al ratio) that will be incorporated in each competing zeolite framework. The results suggest, in agreement with a previous study, that zeolites that are able to incorporate a larger aluminum content (lower Si/Al) are more likely to be synthesized. This arises in part from the larger stability of the incorporation of aluminum with respect to silicon oligomers, coming from the thermodynamics of the synthesis process. The syntheses of aluminosilicate PST-21 (PWO) and PST-22 (PWW) have been explained from the computational results as with higher energy stabilized at excess fluoride conditions than the lowest energy structures, that are obtained at HF/SDA = 1. For the case of ERS-7 (ESV) the justification can only be done if AST is obtained at an intermediate fluoride content between the standard (HF/SDA

= 1) and that corresponding to ESV (HF/SDA = 2). Further experiments not currently available may help to clarify this point.

The computational results also allow splitting of the total energy of the zeolite-SDA system, which is one of the main components of the synthesis energy, into different energetic contributions. From the subsequent analysis, it is possible to quantify, among others, the extent of the zeo-SDA van der Waals contribution, which is well-known to be one of the main contributions to drive the zeolite synthesis. Calculation of this contribution as energy per SDA molecule and as energy per TO_2 atom allowed us to separate the effects of "fitting" and "packing", respectively. The latter includes the former, but it also adds the role of how the zeolite porosity is filled by SDA molecules and relates also to the number of aluminum atoms (Si/Al) that can be incorporated in the zeolite phase.

Further insights into the results of the zeolite synthesis are expected when the role of defects is incorporated in the calculations. This is underway and will be the subject of future studies.

■ ASSOCIATED CONTENT

ⓢ Supporting Information

The Supporting Information is available free of charge at https://pubs.acs.org/doi/10.1021/acs.jpcc.3c03640.

> Details of synthesis; energetic analysis of fluoro-aluminosilicate zeolites; zeo-SDA energies of aluminosilicate and pure-silica zeolites; synthesis energies of aluminosilicate and pure silica zeolites (PDF)

> CIF files with coordinates of all final geometries of aluminosilicate and pure-silica zeo-OSDA systems calculated in this study; CAR files of OSDA molecules used in this study with neutral and cationic charge (ZIP)

■ AUTHOR INFORMATION

Corresponding Author

German Sastre − *Instituto de Tecnologia Quimica UPV/CSIC, Universidad Politecnica de Valencia, 46022 Valencia, Spain;* ⓘ orcid.org/0000-0003-0496-6331; Phone: +34963879445; Email: gsastre@itq.upv.es

Author

Omer F. Altundal − *Instituto de Tecnologia Quimica UPV/CSIC, Universidad Politecnica de Valencia, 46022 Valencia, Spain*

Complete contact information is available at: https://pubs.acs.org/10.1021/acs.jpcc.3c03640

Author Contributions

The manuscript was written through contributions of all authors. All authors have given approval to the final version of the manuscript.

Notes

The authors declare no competing financial interest.

■ ACKNOWLEDGMENTS

■ REFERENCES

(1) Knott, B. C.; Nimlos, C. T.; Robichaud, D. J.; Nimlos, M. R.; Kim, S.; Gounder, R. Consideration of the Aluminum Distribution in Zeolites in Theoretical and Experimental Catalysis Research. *ACS Catal.* 2018, 8 (2), 770−784.

(2) Van Speybroeck, V.; Hemelsoet, K.; Joos, L.; Waroquier, M.; Bell, R. G.; Catlow, C. R. A. Advances in Theory and Their Application within the Field of Zeolite Chemistry. *Chem. Soc. Rev.* 2015, 44 (20), 7044−7111.

(3) Chizallet, C.; Bouchy, C.; Larmier, K.; Pirngruber, G. Molecular Views on Mechanisms of Brønsted Acid-Catalyzed Reactions in Zeolites. *Chem. Rev.* 2023, 123 (9), 6107−6196.

(4) Loewenstein, W. The Distribution of Aluminum in the Tetrahedra of Silicates and Aluminates. *Am. Mineral.* 1954, 39 (1−2), 92−96.

(5) Sato, M.; Maeda, K.; Hirasawa, K. Examination of Dempsey's Rule on the Si,Al Distribution in Zeolite Frameworks. *Chem. Lett.* 1994, 23 (8), 1543−1546.

(6) Sato, M. Hamiltonian Graph Representation of Zeolite Frameworks and Si, Al Ordering in the Framework. *J. Math. Chem.* 1991, 7 (1), 341−352.

(7) Herrero, C. P. Atom Ordering in the Tetrahedral Framework of Zeolite A. *J. Phys.: Condens. Matter* 1993, 5 (25), 4125.

(8) Lippmaa, E.; Maegi, M.; Samoson, A.; Engelhardt, G.; Grimmer, A. R. Structural Studies of Silicates by Solid-State High-Resolution Silicon-29 NMR. *J. Am. Chem. Soc.* 1980, 102 (15), 4889−4893.

(9) Lemishko, T.; Valencia, S.; Rey, F.; Jiménez-Ruiz, M.; Sastre, G. Inelastic Neutron Scattering Study on the Location of Brønsted Acid Sites in High Silica LTA Zeolite. *J. Phys. Chem. C* 2016, 120 (43), 24904−24909.

(10) Lemishko, T.; Jiménez-Ruiz, M.; Rey, F.; Valencia, S.; Blasco, T.; Vidal Moya, A.; Sastre, G. Inelastic Neutron Scattering Study of the Aluminum and Brønsted Site Location in Aluminosilicate LTA Zeolites. *J. Phys. Chem. C* 2018, 122 (21), 11450−11454.

(11) Ahn, S. H.; Wang, Q.; Wang, Y.; Chu, Y.; Deng, F.; Hong, S. B. Identifying Crystallographically Different Si-OH-Al Brønsted Acid Sites in LTA Zeolites. *Angew. Chem., Int. Ed.* 2022, 61 (24), No. e202203603.

(12) Jeffroy, M.; Nieto-Draghi, C.; Boutin, A. New Molecular Simulation Method To Determine Both Aluminum and Cation Location in Cationic Zeolites. *Chem. Mater.* 2017, 29 (2), 513−523.

(13) Sklenak, S.; Dědeček, J.; Li, C.; Wichterlová, B.; Gábová, V.; Sierka, M.; Sauer, J. Aluminum Siting in Silicon-Rich Zeolite Frameworks: A Combined High-Resolution 27Al NMR Spectroscopy and Quantum Mechanics/Molecular Mechanics Study of ZSM-5. *Angew. Chem., Int. Ed.* 2007, 46 (38), 7286−7289.

(14) Yokoi, T.; Mochizuki, H.; Namba, S.; Kondo, J. N.; Tatsumi, T. Control of the Al Distribution in the Framework of ZSM-5 Zeolite and Its Evaluation by Solid-State NMR Technique and Catalytic Properties. *J. Phys. Chem. C* 2015, 119 (27), 15303−15315.

(15) Toyoda, H.; Osuga, R.; Wang, Y.; Park, S.; Yazawa, K.; Gies, H.; Gilbert, C. J.; Yilmaz, B.; Kelkar, C. P.; Yokoi, T. Clarification of Acid Site Location in MSE-Type Zeolites by Spectroscopic Approaches Combined with Catalytic Activity: Comparison between UZM-35 and MCM-68. *Phys. Chem. Chem. Phys.* 2022, 24 (7), 4358−4365.

(16) Li, C.; Vidal-Moya, A.; Miguel, P. J.; Dedecek, J.; Boronat, M.; Corma, A. Selective Introduction of Acid Sites in Different Confined Positions in ZSM-5 and Its Catalytic Implications. *ACS Catal.* 2018, 8 (8), 7688−7697.

(17) Pinar, A. B.; Gómez-Hortigüela, L.; McCusker, L. B.; Pérez-Pariente, J. Controlling the Aluminum Distribution in the Zeolite Ferrierite via the Organic Structure Directing Agent. *Chem. Mater.* 2013, 25 (18), 3654−3661.

(18) Di Iorio, J. R.; Li, S.; Jones, C. B.; Nimlos, C. T.; Wang, Y.; Kunkes, E.; Vattipalli, V.; Prasad, S.; Moini, A.; Schneider, W. F.; Gounder, R. Cooperative and Competitive Occlusion of Organic and Inorganic Structure-Directing Agents within Chabazite Zeolites Influences Their Aluminum Arrangement. *J. Am. Chem. Soc.* 2020, 142 (10), 4807−4819.

(19) Wang, Z.; Chu, W.; Zhao, Z.; Liu, Z.; Chen, H.; Xiao, D.; Gong, K.; Li, F.; Li, X.; Hou, G. The Role of Organic and Inorganic Structure-Directing Agents in Selective Al Substitution of Zeolite. *J. Phys. Chem. Lett.* 2021, 12 (38), 9398−9406.

(20) Li, Y.; Shi, C.; Li, L.; Yang, G.; Li, J.; Xu, J.; Gu, Q.; Wang, X.; Han, J.; Zhang, T.; Li, Y.; Yu, J. Unraveling Templated-Regulated Distribution of Isolated SiO4 Tetrahedra in Silicoaluminophosphate Zeolites with High-Throughput Computations. *Natl. Sci.* 2022, 9 (9), nwac094.

(21) Tang, X.; Chen, W.; Dong, W.; Liu, Z.; Yuan, J.; Xia, H.; Yi, X.; Zheng, A. Framework Aluminum Distribution in ZSM-5 Zeolite Directed by Organic Structure-Directing Agents: A Theoretical Investigation. *Catal. Today* 2022, 405−406, 101−110.

(22) Rabdel Ruiz-Salvador, A; Gomez, A.; Lewis, D. W.; Rodriguez-Fuentes, G.; Montero, L. Silicon-Aluminium Distribution in Dehydrated Calcium Heulandite. *Phys. Chem. Chem. Phys.* 1999, 1 (7), 1679−1685.

(23) Jones, A. J.; Carr, R. T.; Zones, S. I.; Iglesia, E. Acid Strength and Solvation in Catalysis by MFI Zeolites and Effects of the Identity, Concentration and Location of Framework Heteroatoms. *J. Catal.* 2014, 312, 58−68.

(24) Perea, D. E.; Arslan, I.; Liu, J.; Ristanović, Z.; Kovarik, L.; Arey, B. W.; Lercher, J. A.; Bare, S. R.; Weckhuysen, B. M. Determining the Location and Nearest Neighbours of Aluminium in Zeolites with Atom Probe Tomography. *Nat. Commun.* 2015, 6 (1), 7589.

(25) Ghorbanpour, A.; Rimer, J. D.; Grabow, L. C. Periodic, VdW-Corrected Density Functional Theory Investigation of the Effect of Al Siting in H-ZSM-5 on Chemisorption Properties and Site-Specific Acidity. *Catal. Comm.* 2014, 52, 98−102.

(26) Berkson, Z. J.; Hsieh, M.-F.; Smeets, S.; Gajan, D.; Lund, A.; Lesage, A.; Xie, D.; Zones, S. I.; McCusker, L. B.; Baerlocher, C.; Chmelka, B. F. Preferential Siting of Aluminum Heteroatoms in the Zeolite Catalyst Al-SSZ-70. *Angew. Chem., Int. Ed.* 2019, 58 (19), 6255−6259.

(27) Shantz, D. F.; Lobo, R. F.; Fild, C.; Koller, H. Controlling the Distribution of Framework Aluminum in High-Silica Zeolites. In *Stud. Surf. Sci. Catal.*; Corma, A., Melo, F. V., Mendioroz, S., Fierro, J. L. G., Eds.; 12th International Congress on Catalysis; Elsevier, 2000; Vol. 130, pp 845−850.

(28) Sabater, M. J.; Sastre, G. A Computational Study on the Templating Ability of the Trispyrrolidinium Cation in the Synthesis of ZSM-18 Zeolite. *Chem. Mater.* 2001, 13 (12), 4520−4526.

(29) Sastre, G.; Fornes, V.; Corma, A. On the Preferential Location of Al and Proton Siting in Zeolites: A Computational and Infrared Study. *J. Phys. Chem. B* 2002, 106 (3), 701−708.

(30) Wang, X.; Wang, Y.; Moini, A.; Gounder, R.; Maginn, E. J.; Schneider, W. F. Influence of an N,N,N-Trimethyl-1-Adamantyl Ammonium (TMAda+) Structure Directing Agent on Al Distributions and Pair Features in Chabazite Zeolite. *Chem. Mater.* 2022, 34 (24), 10811−10822.

(31) Rubeš, M.; Trachta, M.; Vaculík, J.; Bulánek, R.; Bludský, O. The Analysis of the BAS OH Band in Zeolites. *Microporous Mesoporous Mater.* 2022, 341, 112052.

(32) Muraoka, K.; Chaikittisilp, W.; Yanaba, Y.; Yoshikawa, T.; Okubo, T. Directing Aluminum Atoms into Energetically Favorable Tetrahedral Sites in a Zeolite Framework by Using Organic Structure-Directing Agents. *Angew. Chem., Int. Ed.* 2018, 57 (14), 3742−3746.

(33) Antúnez-García, J.; Galván, D. H.; Petranovskii, V.; Murrieta-Rico, F. N.; Yocupicio-Gaxiola, R. I.; Shelyapina, M. G.; Fuentes-Moyado, S. Aluminum Distribution in Mordenite-Zeolite Framework: A New Outlook Based on Density Functional Theory Calculations. *J. Solid State Chem.* 2022, 306, 122725.

(34) Lew, C. M.; Xie, D.; Schmidt, J. E.; Elomari, S.; Davis, T. M.; Zones, S. I. The Confluence of Organo-Cations, Inorganic Species, and Molecular Modeling on the Discovery of New Zeolite Structures and Compositions. *AI-Guided Design and Property Prediction for Zeolites and Nanoporous Materials*; John Wiley & Sons, Ltd., 2023; pp 1−32.

(35) Daeyaert, F.; Deem, M. De Novo Design of Organic Structure Directing Agents for the Synthesis of Zeolites. *AI-Guided Design and*

Property Prediction for Zeolites and Nanoporous Materials; John Wiley & Sons, Ltd., 2023; pp 33−59.

(36) Isaac, C.; Deroche, I.; Paillaud, J.-L.; Daou, T. J.; Ryzhikov, A.; Michelin, L.; Rigolet, S.; Josien, L.; Nouali, H. All-Silica SSZ-74 Synthesized in Fluoride or Fluoride-Free Media: Investigation on Organic Structure-Directing Agent's Locations Inside Pores. *Cryst. Growth Des.* **2021**, *21* (7), 4013−4022.

(37) Sastre, G.; Leiva, S.; Sabater, M. J.; Gimenez, I.; Rey, F.; Valencia, S.; Corma, A. Computational and Experimental Approach to the Role of Structure-Directing Agents in the Synthesis of Zeolites: The Case of Cyclohexyl Alkyl Pyrrolidinium Salts in the Synthesis of *β*, EU-1, ZSM-11, and ZSM-12 Zeolites. *J. Phys. Chem. B* **2003**, *107* (23), 5432−5440.

(38) Bae, J.; Dusselier, M. Synthesis Strategies to Control the Al Distribution in Zeolites: Thermodynamic and Kinetic Aspects. *Chem. Commun.* **2023**, *59* (7), 852−867.

(39) Leon, S.; Sastre, G. Zeolite Phase Selectivity Using the Same Organic Structure-Directing Agent in Fluoride and Hydroxide Media. *J. Phys. Chem. C* **2022**, *126* (4), 2078−2087.

(40) Altundal, O. F.; Leon, S.; Sastre, G. Different Zeolite Phases Obtained with the Same Organic Structure Directing Agent in the Presence and Absence of Aluminum: The Directing Role of Aluminum in the Synthesis of Zeolites. *J. Phys. Chem. C* **2023**, *127* (22), 10797−10805.

(41) Jo, D.; Park, G. T.; Shin, J.; Hong, S. B. A Zeolite Family Nonjointly Built from the 1,3-Stellated Cubic Building Unit. *Angew. Chem., Int. Ed.* **2018**, *57* (8), 2199−2203.

(42) Bae, J.; Hong, S. B. Choline-Mediated Synthesis of Zeolite ERS-7 via an Excess Fluoride Approach. *Chem. Commun.* **2018**, *54* (78), 10997−11000.

(43) Baerlocher, Ch.; McCusker, L. B. *Database of Zeolite Structures*; 2022; http://www.iza-structure.org/databases/.

(44) Schwalbe-Koda, D.; Santiago-Reyes, O. A.; Corma, A.; Román-Leshkov, Y.; Moliner, M.; Gómez-Bombarelli, R. Repurposing Templates for Zeolite Synthesis from Simulations and Data Mining. *Chem. Mater.* **2022**, *34* (12), 5366−5376.

(45) Gálvez-Llompart, M.; Cantín, A.; Rey, F.; Sastre, G. Computational Screening of Structure Directing Agents for the Synthesis of Zeolites. A Simplified Model. *Z. Kristallogr. - Cryst. Mater.* **2019**, *234* (7−8), 451−460.

(46) Gale, J. D. GULP: A Computer Program for the Symmetry-Adapted Simulation of Solids. *J. Chem. Soc., Faraday Trans.* **1997**, *93* (4), 629−637.

(47) Oie, T.; Maggiora, G. M.; Christoffersen, R. E.; Duchamp, D. J. Development of a Flexible Intra- and Intermolecular Empirical Potential Function for Large Molecular Systems. *Int. J. Quantum Chem.* **1981**, *20* (S8), 1−47.

(48) Rappe, A. K.; Casewit, C. J.; Colwell, K. S.; Goddard, W. A. I.; Skiff, W. M. UFF, a Full Periodic Table Force Field for Molecular Mechanics and Molecular Dynamics Simulations. *J. Am. Chem. Soc.* **1992**, *114* (25), 10024−10035.

(49) Bushuev, Y. G.; Sastre, G. Atomistic Simulations of Structural Defects and Water Occluded in SSZ-74 Zeolite. *J. Phys. Chem. C* **2009**, *113* (25), 10877−10886.

(50) Ewald, P. P. Die Berechnung Optischer Und Elektrostatischer Gitterpotentiale. *Ann. Phys.* **1921**, *369* (3), 253−287.

(51) Bae, J.; Hong, S. B. Zeolite Synthesis by the Excess Fluoride Approach in the Presence of Piperidinium-Based Structure-Directing Agents. *Microporous Mesoporous Mater.* **2021**, *327*, 111422.

(52) Rojas, A.; Martínez-Morales, E.; Zicovich-Wilson, C. M.; Camblor, M. A. Zeolite Synthesis in Fluoride Media: Structure Direction toward ITW by Small Methylimidazolium Cations. *J. Am. Chem. Soc.* **2012**, *134* (4), 2255−2263.

(53) Zicovich-Wilson, C. M.; San-Román, M. L.; Camblor, M. A.; Pascale, F.; Durand-Niconoff, J. S. Structure, Vibrational Analysis, and Insights into Host-Guest Interactions in As-Synthesized Pure Silica ITQ-12 Zeolite by Periodic B3LYP Calculations. *J. Am. Chem. Soc.* **2007**, *129* (37), 11512−11523.

(54) Moteki, T.; Lobo, R. F. A General Method for Aluminum Incorporation into High-Silica Zeolites Prepared in Fluoride Media. *Chem. Mater.* **2016**, *28* (2), 638−649.

(55) Lee, Y.; Park, M. B.; Kim, P. S.; Vicente, A.; Fernandez, C.; Nam, I.-S.; Hong, S. B. Synthesis and Catalytic Behavior of Ferrierite Zeolite Nanoneedles. *ACS Catal.* **2013**, *3* (4), 617−621.

(56) Misturini, A.; Altundal, O. F.; García-Aznar, P.; Kariminasab, S.; Sastre, G. Effect of Intracrystalline Silanol Defects on the Diffusivity of Benzene in Silicalite Zeolite. *Chem. Ing. Technol.* **2023**, DOI: 10.1002/cite.202300008.

(57) Bertolazzo, A. A.; Dhabal, D.; Molinero, V. Polymorph Selection in Zeolite Synthesis Occurs after Nucleation. *J. Phys. Chem. Lett.* **2022**, *13* (4), 977−981.

(58) Kumar, A.; Nguyen, A. H.; Okumu, R.; Shepherd, T. D.; Molinero, V. Could Mesophases Play a Role in the Nucleation and Polymorph Selection of Zeolites? *J. Am. Chem. Soc.* **2018**, *140* (47), 16071−16086.